Proceedings of the ASME Pressure Vessels & Piping PVP 2008 Conference
July 27- 31, 2008, Chicago, Ill USA

PVP 2008-61247

WELD RESIDUAL STRESS AND DISTORTION ANALYSIS OF THE ARES I-X UPPER STAGE SIMULATOR (USS)

Frederick W. Brust
Engineering Mechanics Corporation of Columbus (EMC^2)
Columbus, OH, USA

Ivatury Raju
NASA Engineering and Safety Center (NESC)
NASA Langley Research Center (LARC)
Hampton, VA, USA

Derrick Cheston
NASA Engineering and Safety Center (NESC)
NASA Glenn Research Center
Cleveland, OH, USA

David Dawicke
Analytical Services & Materials, Inc.
Hampton, VA, USA

Dawn Phillips
Lockheed Martin
Hampton, VA, USA

ABSTRACT

An independent assessment was conducted to determine the critical initial flaw size (CIFS) for the flange-to-skin weld in the Ares I-X Upper Stage Simulator (USS). The Ares system of space launch vehicles is the US National Aeronautics and Space Administration's plan for replacement of the aging space shuttle. The new Ares space launch system is somewhat of a combination of the space shuttle system and the Saturn launch vehicles used prior to the shuttle. Here, a series of weld analyses are performed to determine the residual stresses in a critical region of the USS. Weld residual stresses both increase constraint and mean stress thereby having an important effect on fatigue and fracture life. While the main focus of this paper is a discussion of the weld modeling procedures and results for the USS, a short summary of the CIFS assessment is provided.

INTRODUCTION

The NASA safety standard for human spaceflight requires that critical structural components be designed so that the largest crack that can be missed by the appropriated NDE technique does not grow to a critical length within four lifetimes. Fracture mechanics must be used to analytically determine the maximum initial crack or flaw size that would not produce a critical stress intensity factor in the location of concern after four simulated life cycles. This critical initial flaw size is referred to as the CIFS.

The Ares I-X (AIX) Upper Stage Simulator (USS) represents the upper stage of the Ares I vehicle in mass, center-of-gravity, and outer mold line. To achieve a low manufacturing cost, the AIX inert upper stage is designed in a modular fashion consisting of cylindrical segments that are made of construction grade A516 Grade 70 12.7 mm (½-inch) plate steel with machined flanges welded onto either end for bolting adjacent segments. Keep in mind that this assessment is being made for the simulator only and will not be the flight material.

The flange-to-skin or flange-to-shell weld is one of several weld joints used in the design of the USS. The flange-to-skin weld is located at the outermost diameter of the upper stage simulator and is in the primary load path of the flight test vehicle (Figure 1). The USS consists of several "tuna can" segments that are approximately 5.5 m in diameter, 2.9 m inches tall, and 12.7 mm thick. A 152 mm wide by 25.4 mm thick flange is welded to the skin and is used to fasten adjacent tuna cans. Gussets are welded to the skin and flange every 10 degrees around the circumference of the "tuna can". The flange-to-skin weld is a flux core butt weld with a fillet weld on the inside surface. The welding process often creates loss of fusion defects in the weld that could develop into fatigue cracks and jeopardize the structural integrity of the Ares I-X vehicle.

A CIFS assessment was made for the welds within the common segments designated US-1 through US-7 whose shell and flange designs were identical. The US-1/US-2 interface flange-to-skin welds were chosen for the analysis because they experience the highest service loads. This weld represents a rather unique geometry, which cannot be modeled using an axis-symmetric model. Moreover, the geometry is quite different from typical 'pipe or cylinder' type welds and the results are not necessarily intuitive.

In this paper the main features of the weld analysis are discussed and a brief summary of the CIFS assessment is provided. The purpose of this set of weld analyses is to model the weld process using a variety of sequences to determine the 'best' sequence in terms of weld residual stresses and distortions. The many factors examined in this study include weld design (single-vee, double-vee groove), weld sequence, boundary conditions, and material properties, among others. In addition, mesh refinement studies are included. Full three dimensional weld analyses are performed. The results of this weld analysis are included with service loads (including fit-up stresses) to perform a fatigue and critical initial flaw size evaluation.

WELD ANALYSIS PROCEDURE

Computational weld modeling is challenging because many of the processes of welding are highly nonlinear. Material melts and re-solidifies, very high transient thermal gradients are experienced, non-linear temperature dependent plastic straining and phase transformations can occur, among other sources of nonlinearity. Moreover, for weld modeling to have practical advantages in industrial production, computational solution times must be manageable since an optimum weld design of large, complex fabrications requires numerous separate analyses.

Most computational weld models that are available commercially are mathematics and physics based models. The following is a brief description of the VFT™ (Virtual Fabrication Technology, VFT, (Reference [1]) code. Other codes are also available for predicting and controlling weld residual stresses and distortions. There are two main analysis modules, the thermal model and the structural model, that make up the weld process simulation methodology in VFT that are briefly summarized below. Welding distortion simulation normally adopts sequentially coupled thermal structural analysis. First, the thermal analysis is performed. Then the structural analysis is performed using the temperatures predicted by the thermal analysis as the thermal load in conjunction with any additional mechanical loads or constraints. Material response in a welding process is very much localized along the welds. For large fabricated structures, the simulations involve millions of degrees of freedom and are highly nonlinear, and hence are extremely computationally intensive. As such, coarse meshes must be used for the global distortion predictions. However, numerical thermal predictions using such coarse meshes are inadequate, especially for capturing the thermal gradients and cooling rates during welding processes. Developing efficient and effective simulation procedures that take into account these contrasting

requirements is crucial to practically and successfully applying welding simulations to large problems.

Thermal Solutions and CTSP. The thermal model (CTSP) was developed based on superposition of complicated closed form analytical expressions and developed heat source theories. CTSP is very rapid and is used for large problems. Numerical thermal solutions based on a modification of Goldak theory are also used, but these solutions often take a long time to perform for large problems. The CTSP solutions were used here because they have been shown to be very accurate for large problems and solution times are on the order of several minutes compared with hours and days for a full numerical thermal solution.

Comprehensive Thermal Solution Procedure (CTSP) [4, 5, 8-10] is a closed form solution thermal analysis code specifically developed for global distortion and residual stress prediction of production components such as the Ares 1-X. The code is an analytical solution based on the Rosenthal solution of a point heat source moving in an infinite domain at a constant direction and speed. Without additional treatment, the Rosenthal solution cannot be used to calculate the temperature profiles for industrial applications. To simulate the surface of a component, CTSP uses the imaginary heat sources reflected on the surface of the component to achieve the equivalent heat conduction. Meanwhile, CTSP uses the "negative" heat sources starting at the time of welding end to simulate the stop of the welding and transients (see [8-10]).

Using these techniques, CTSP is able to simulate typical weld joint types such as groove joints, lap joints, T-fillet joints, traverse complex welds, and multiple weld paths. Figure 2 shows the validation of CTSP against the experimental measurement. This example is for a tee-fillet weld similar to the ARES weld models to be discussed later. During the development of the VFT code, numerous validation examples were used to drive the code development (many can be found in References [1-10] and the many references sited therein). These validations were made with both thermocouple measurements of test components and full numerical thermal solutions using DFLUX user routines in conjunction with the commercial finite element analysis code ABAQUS®. The details on CTSP have been well documented and reported in the literature. Only its advantage and essential features are highlighted as follows.

- The computation time for CTSP is much faster than that of a numerical solution. Depending on the complexity of the structure, a thermal calculation using CTSP can be 100~1000 times faster than a finite element analysis. One reason for this significant speedup is that CTSP avoids the calculation of the whole structure and only focuses on the local region around the heat-affected zone.
- CTSP solutions for coarse meshes are very accurate for predicting the temperatures at the coarse node points. These temperatures provide accurate through thickness temperatures, which are critical as input for providing accurate distortion and residual stress predictions.

Perhaps the only area where a numerical solution has an advantage compared with CTSP is cases where the material micro-structure needs to be predicted as modified by welding.

Structural Solution and Weld Constitutive Model. The structural model (UMAT) was developed based on ABAQUS commercial finite element codes by implementing a special materials module, which includes a constitutive law that permits stress relief due to weld melting/re-melting effects, strain hardening effects, large deformation mechanisms, rapid weld metal deposition features, phase transformation plasticity (based on the Leblond model [Ref. 2]), etc. Experience clearly suggests that uncoupled thermal/structural solutions for weld problems is accurate in all weld models. Moreover, visco-plastic (or creep) effects are not important since the time spent in the creep regime during welding is negligible. However, creep effects are permitted and are often used to model heat treatments of steels and stress relief due to heat treatment. The constitutive model library within the UMAT permits isotropic, kinematic, and mixed hardening (Lemaitre-Chaboche). Here isotropic hardening is used, which tends to produce upper bound stress results. Many more details of the VFT code, with many example solutions, can be found in References [1 -10] and in the many references therein.

ARES 1-X WELD MODELING RESULTS

The key Ares I-X weld and corresponding results are presented in this section. During this work there were a number of different weld concepts, procedures, and joint types considered. Many of these analyses are omitted here to focus on the important results (see Reference [11] for details). Suffice it to say that many of the weld concepts were rejected because the residual stress field produced was not advantageous. In general, it was found that minimizing the weld residual stresses near the inner diameter of the shell-to-flange weld resulted in the largest critical initial flaw size (CIFS).

The heat and corresponding weld shrinkage caused by welding lead to residual stresses. These residual stresses are localized to the region of the weld. The residual stresses also cause distortions that can affect fit up and tolerance requirements throughout the component structure. The residual stresses in the shell and flange prior to welding were not considered in this analysis although in some cases these can be important [12].

Formatted: Bullets and Numbering

Weld Geometry. A ten-degree segment of the tuna can shell and flange was modeled as shown in Figure 3. To reduce the solution degree-of-freedoms a 96 cm length of the can was chosen for analysis and the remainder of the acreage of the can was omitted. The can was modeled with ABAQUS C3DR solid elements. A gusset with a 'mouse hole' was included to capture the correct stiffness. In the model, the gusset weld itself was not explicitly modeled. Because of the presence of the gusset, the problem is not axis-symmetric. However, some axis-symmetric analyses were performed during sensitivity studies. The boundary conditions shown in the left hand side

of Figure 3 were chosen to prohibit rigid body motion of the flange ring segment during the weld process. At both ends of the model (0- and 10-degree locations), free boundary conditions were imposed. Two sets of analyses were performed to verify the local nature of the web residual stresses. One analysis was performed where cyclic symmetry boundary conditions were imposed at the 0- and 10-degree locations. Another analysis was performed where the omitted acreage of the can was included and modeled with shell elements. As expected, the weld residual stress influence was local to the weld joint and hence neither the cyclic boundary conditions nor inclusion of the acreage of the can had an important effect on weld residual stress. Finally, as seen in the right of Figure 3 three meshes of increasing refinement were used to verify that the solution converged (the course, fine, and finest models, respectively). The model labeled 'finest model' was used for the analyses that were used for the final CIFS solutions.

The inset of Figure 3 shows the details of the weld joint. The joint was either a single-vee or a 'double-vee' with a fillet weld deposited along the inner diameter of the shell- surface interface. The thick flange ring stiffness and the gusset had a profound influence on the weld residual stresses compared to a simple shell groove weld (as in a large diameter pipe). The welds were made using 5 to 7 weld passes depending on the sequence. The weld parameters were: Amps = 200- 215, Volts = 25 – 26, and weld speed = 4 – 5 mm/sec. The thermo-physical properties used for the thermal analysis and the temperature dependent stress strain curves used for A516-70 steel are presented in references 13and 14. Full moving arc analyses were performed since 'lump pass' assumptions, where the passes are deposited at once, were found to produce less accurate results.

Figure 4 illustrates the locations where the weld residual stresses were compiled and used in the critical initial flaw size (CIFS) evaluations. As seen in the lower left insert, the stresses were evaluated in the shell at the toe of the fillet weld from the ID to OD of the shell. Axial (perpendicular to the weld direction) and hoop (the weld travel direction) residual stresses were compiled at locations illustrated in Figure 4. Cut plane 0 runs through the first full hole, cut plane 1 is through the second hole, cut plane 2 is at the gusset 'mouse hole' location, and cut plane 3 is on the other side of the gusset near the weld stop location as illustrated in Figure 4. The stresses at other locations (including the possibility of cracks in the ring) were also considered for the CIFS analysis but it was determined that circumferential crack growth (caused by axial shell stresses at the toe of the weld) were most critical. More details of this analysis can be found in [11, 12, and 15].

Weld Sequences. There are a number of factors that determine the final weld residual stress and distortion state. Weld modeling is often used to design weld methods to either minimize or control residual stresses and/or distortions. Some of the many techniques that have been developed are discussed in detail in Reference [5]. Some of these factors include weld sequence, weld groove geometry, weld parameters, weld piece constraint, tacking methods, use of heat sinks, thermal tensioning, weld electrode used, and special methods such as pre-cambering, pre-bend, post weld heat treat, among many others. For the ARES I-X work considered here, the weld groove geometry and weld sequence were key contributing factors in developing a favorable or unfavorable weld residual stress state. The weld definitions and weld sequences presented here were mainly driven by the NASA program team. A key conclusion from this weld modeling work, which is discussed in detail later, is that the final pass should be deposited at the outer diameter (OD) of the shell to flange weld. For both joint geometries (single and double-vee) shown in Figure 5, the weld sequences in Figure 5 a, b, and d should be used and the Figure 5c sequence should be avoided. Note that the weld passes here are idealized with square elements. This has a second order effect on the final residual stress pattern [11]. As discussed in [11] the Figure 5c sequence results in a high tensile weld residual state at the ID of the shell. This results in reduced fatigue life and a smaller CIFS.

The original weld sequence shown in Figure 5a was single-vee weld geometry. The fillet weld is deposited first and then the weld joint is sequentially filled from the ID to the OD. This type of weld joint will typically result in larger out of plane weld distortions since the weld shrinkage progresses from the ID to OD as each pass is deposited. Figure 5 (b-d) shows the weld sequence for a balanced double-vee weld. It is seen that the weld is balanced about the mid thickness of the shell, which tends to minimize distortions in such welds.

Weld Residual Stresses. Figure 6 illustrates the Von Mises and Axial weld residual stress profiles for the double-vee weld sequence. The stresses vary with position because of the moving weld arc, the stiffness supplied by the gusset, and to some extent, the holes in the flange. Figure 7 shows the axial weld residual stresses at each of the four cut locations. The axial stresses at cut locations 1 and 2 are largest in magnitude. Figure 8 is a plot of the weld residual stresses at the four cut locations in the finest model. These are axial stresses plotted from the shell inner diameter through the wall thickness (12.7 mm or 0.5-inch) at the fillet weld toe as illustrated in the inset of Figure 8. These are the stresses that are used for the CIFS analyses. Axial stresses can contribute to circumferential cracks in the shell at the toe of the fillet, which is the key concern for the tuna can shell welds.

The tuna can weld analysis of the double-vee geometry was performed using three different mesh refinements. This was done for two reasons: (i) to ensure the solution converged and (ii) to ensure there were no solution errors since the analyses were performed separately and independently. There were some differences in the weld residual stress magnitudes using the different mesh refinements [11], but the stress patterns were very similar. The results from the finest mesh solution were used for the CIFS analysis.

As a simple rule of thumb regarding weld analyses for cases where there are not many weld passes (here only 6 total passes), the final weld beads tend to control the location of

axial tensile weld residual stresses. (The 'hoop' weld residual stresses in the direction of welding are usually fully tensile for shells of this thickness). This is illustrated in Figure 9, where the axial weld residual stresses for passes 3 to 6 are illustrated at the cut-2 location using the finest finite element model. The weld sequence is illustrated in the left inset of Figure 9. One can see that after passes 3 and 5 are complete, the tensile axial stresses are on the inside diameter of the shell. After passes 4 and 6, the tensile stresses move to the outer diameter.

Pipe Weld Versus Area I-X Weld. The results shown here are now compared to what would be expected in a shell weld without the ring flange stiffener. In the absence of the ring flange and the gusset the configuration would be analogous to a large diameter girth welded vessel. For a shell of this thickness (12.7 mm), the welding of a pipe would produce tensile weld residual stresses on the shell inner surface (see [11] for details). This is caused by two competing mechanisms. The radial shrinkage of the weld bead is like applying a 'ring load' to the pipe, which produces bending stresses through the shell wall – tension at the ID and compression at the OD. On the other hand, the axial shrinkage of the weld bead tends to produce axial tension at the location of the weld. For a weld sequence as in Figure 5c, where the last pass is deposited at the OD, this axial shrinkage would result in tension. Hence in a shell, there is a competition between radial and axial shrinkage. In a shell of this thickness, the bending type deformation dominates, resulting in tension at the ID and compression at the OD. For the Ares I-X vehicle, compression results at the ID, compression in the middle with a small amount of tension at the OD as shown in Figures 8 and 9. This is the result of the additional competition of the stiff flange ring and the gusset. As such, the weld residual stress distribution in the Ares I-X is not intuitive. A number of other studies, including some axis-symmetric were performed examining, and are presented in reference 11.

Weld Constraint and Fracture. The weld process can produce a residual stress state in the weld joint that increases the constraint thereby reducing fracture toughness. It is well known that plane strain fracture toughness is lower than plane stress because the amount of plasticity that can develop under plane strain conditions is reduced. The development of direct relationships between constraint and fracture toughness is a topic of fruitful research at present in the fracture community. However, it is known that for a given material the higher the tensile constraint in the joint the lower the toughness. Figure 10 shows the constraint (hydrostatic stress measured as $s_{kk}/3$, where s_{ij} represents the stress tensor) and the von Mises stress through the shell at the cut-2 location. It is clear that there is significant tensile constraint near the mid thickness of the shell. Because yielding in metals is independent of hydrostatic stress it is possible for the component stresses to be higher than yield (sometimes significantly). The hoop stresses are higher than the room temperature yield stress of 345 MPa (50 ksi). The maximum von Mises stress at this location is 483 MPa, the hydrostatic stress is 323 MPa, and the hoop stress is 600 Mpa at $x/t = 0.5$.

Weld Sequence and Load Shakedown. Figure 11 illustrates the importance of weld sequence in determining the final weld residual stress pattern for the tuna can shell-to-flange weld. The balanced sequence for the double-vee weld case is shown in the upper right insert. This balanced type of weld sequence will tend to minimize weld distortions. A weld sequence is shown in the lower right where the outside diameter welds are performed first followed by the inside welds. From Figure 11 it is seen that the axial weld residual stresses change from compression on the inner diameter (ID) for the balanced sequence to tension on the ID for sequence 2. The hoop stresses are also affected. The crack growth is expected to be different for these two markedly different weld residual stress patterns.

Load Shakedown. The service loads that are applied after weld fabrication will often cause the weld residual stresses to 'shakedown' to lower values over time. This effect is examined here for the tuna can shell-to-flange weld. The modeling process is briefly described below and discussed in detail in reference 11.

- Perform the weld analysis. Here the double-vee geometry with the balanced weld sequence was used.
- Add additional boundary conditions to represent the constraint applied to the top of the bolt holes in the pressure load direction. Here displacements were applied such that the value of the displacement after welding was complete was maintained and held constant, i.e., no additional displacement was permitted after application and removal of the load. This was done to simulate the bolt constraints. Note that the weld process induces distortions in the flange. For one analysis (not shown here) these distortions in the flange were eliminated (or made zero) prior to adding the pressure load. This simulates fit up constraints that may occur due to tightening the bolts prior to load application. This has a marked effect on the final weld residual stress state and could be included in another analysis in the future. Results are not shown here because the present model is not considered accurate enough to account for these bolt loads at this point.
- Apply the pressure load and then release the load. Here two pressures (22 MPa (3.2 ksi) and 86 MPa (12.5 ksi)) were applied and released. Since these were applied after the weld modeling was complete, the complete history of welding stresses and strains were properly included in this analysis. The 22 MPa pressure represents an equivalent pressure determined as part of the CIFS analysis cases, and represents a typical maximum service load during space launch.

It was evident that the application of the equivalent pressure of 22 MPa does reduce the final residual stress pattern slightly. One could imagine that if many cycles were applied, and some plasticity occurs locally near the weld during each load cycle, the weld residual stresses would shake down further. The application and release of the 86 MPa pressure load reduces the weld residual stresses at this location

significantly. This may suggest that the application of a 'proof load' to reduce the weld residual stress state in the shell-to-flange weld might be worthy of consideration. Indeed, proof loads applied to nuclear piping systems perform the same function. For the CIFS analysis, shakedown was conservatively ignored.

CRITICAL INITIAL FLAW SIZE EVALUATION (CIFS)

The CIFS analysis was conducted to determine the largest crack in the weld region that will not grow to failure within 4 lifetimes, which is a NASA manned space flight specification. For usual aerospace applications, the NASA life requirement is applied to fatigue assessments that only consider notch effects. However, typical fatigue analyses are inadequate to assess life when defects such as weld defects exist. For structures containing welding defects, the fatigue life requirement needs to be addressed by damage tolerance methodology.

A CIFS analysis assumes an initial crack size (a_i) and grows that crack according to the material behavior (fatigue crack growth rate and fracture toughness), loading spectrum for the structure, and the stress intensity factor for the crack configuration. The critical flaw size (a_{CFS}) is obtained when the maximum stress intensity factor for any one cycle of the loading spectrum exceeds the fracture toughness value. The number of spectrum repeats necessary to grow the crack from a_i to a_{CFS} is N_c. The CIFS crack length (a_{CIFS}) is defined as the largest crack length that will survive 4 repeats of the spectrum, as illustrated in Figure 12. A CIFS analysis requires the following information, and additional details are presented in Reference [15]:

- Loading spectrum [16]. The load spectrum is complicated and includes pad roll-out loads, lift-off, vibration, etc.
- Crack shape, size, and the Stress-intensity factor solution
- Material behavior that describes the fatigue crack growth rate
- Material behavior that describes the critical stress intensity factor
- A fatigue crack growth rate code

The CIFS analysis used linear elastic fracture mechanics assumptions to predict the fatigue crack growth rate of surface and embedded cracks in the inside (ID) and outside (OD) surfaces of the flange-to-skin weld. The analyses used a number of assumptions, the majority of which were very conservative, to account for the unknowns and uncertainties of the problem. The analyses considered four different mean stress assumptions to account for the weld residual stresses and fit-up stresses:

- Constant mean stress of the flow stress (372 MPa) to account for the weld residual stresses and fit-up stresses. This is sometimes assumed if weld residual stress analyses are not available. This is very conservative since the axial weld residual stresses will not be constant through the shell wall thickness at the toe of the weld.
- Residual stresses calculated from a 6-pass weld sequence with the last pass on the ID and the worst case fit-up stresses (largest fit-up stresses calculated with the largest mismatch in the flange flatness). See Figure 5b with passes 5 and 6 reversed.
- Residual stresses calculated from a 7-pass weld sequence with the last pass on the ID and the worst case fit-up stresses (Figure 5c).
- Residual stresses calculated from a 7-pass weld sequence with the last pass on the OD and the worst case fit-up stresses (Figure 5d).

The CIFS results for each of the mean stress assumptions are shown in Figure 13. The assumption of the mean stress equal to the flow stress (372 Mpa) provided the lowest bound on the CIFS for all cases except for ID cracks in the 7-pass weld sequence with the last pass on the OD. The 7-pass weld sequence with the last pass on the OD resulted in high tensile residual stresses on the ID surface. Neglecting the compressive components of the weld residual stresses had no influence on the CIFS for 5 of the 8 combinations of crack location and mean stress assumption and provided a lower CIFS for the other 3 combinations.

SUMMARY

This paper discussed the development of weld residual stresses in the Ares I-X space shuttle replacement and the important effect weld residual stresses have on the critical initial flaw size. It is clear that careful design of weld fabrication procedures, including joint type, weld parameters, weld sequence, fabrication constraints, and distortions are very important to improve the life of welded fabrications.

ACKNOWLEDGMENTS

The authors would like to thank the US National Aeronautics and Space Administration for their careful assessment requirements for space flight.

REFERENCES

1. User Manual for VFT – Virtual Fabrication and Weld Modeling Software by Battelle Memorial Institute and Caterpillar Inc., February 2005.
2. Oh, J., and Brust, F. W., 'Phase Transformation Effects on Weld Distortion and Residual Stress Predictions', in Proceedings of PVP2005, 2005 ASME Pressure Vessels and Piping Division Conference, July 17-21, 2005, Denver, Colorado USA, In *Welding and Residual Stresses*, edited by O'Dowd, N., Brust, F. W., Keim, E., Sherry, A., and Dong, P.
3. Brust, F. W., Yang, Y. Y., Ezeilo, A., and McPherson, N., '*Weld Modeling of Thin Structures With VFT'*, Proceedings of ASME Pressure Vessel and Piping Conference, San Diego, CA, July, 2004, in *Residual Stress, Fracture, and*

Stress Corrosion Cracking, Principal Editor, Y. Y. Wang, 2004.
4. Chen, X. L., Yang, Z, and Brust, F. W., "Modeling Distortion and Residual Stress During Welding", Chapter 7 in *Processes and Mechanisms of Welding Residual Stress and Distortion*, pp. 225 – 263, Woodhead Publishing, July 2005.
5. Brust, F. W., and Kim, D., "Mitigating Welding Residual Stress and Distortion", Chapter 8 in *Processes and Mechanisms of Welding Residual Stress and Distortion*, pp. 264 – 294, Woodhead Publishing, July 2005.
6. Brust, F. W., and Scott, P. M., "Weld Residual Stresses and Primary Water Stress Corrosion Cracking in Bimetal Nuclear Pipe Welds", PVP 2007-26297, Proceedings of the ASME PVP 2007/Creep 8 Conference, ASME, July 22 - 26, 2007, San Antonio, Texas USA.
7. Scott, P. M., Brust, F. W., et al, "The Battelle Integrity of Nuclear Piping (BINP) Final Report", Nuclear Regulatory Commission Report NUREG/CR-6837, Vol. 1 and 2, Prepared by Battelle and Engineering Mechanics Corp., June, 2005.
8. Feng, Z., (Editor), "Processes and Mechanisms of Welding Residual Stress and Distortion" Woodhead Publishing Company, Cambridge, UK, 2005.
9. Cao, Z. Brust, F. W., Nanjundan, A., Dong, Y., and Jutla, T., "A Comprehensive Thermal Solution Procedure for Different Weld Joints", Advances in Computational Engineering and Sciences; ed. S. N. Atluri and F. W. Brust, Tech Science Press, pp 630-636, August, 2000.
10. Brust, F. W., Jutla, T., Yang, Y., Cao, Z., Dong, Y., Nanjundan, A., Chen, X. L., Advances in Computational Engineering and Sciences; ed. S. N. Atluri and F. W. Brust, Tech Science Press, pp 630-636, August, 2000. Also, Numerous Weld Papers in this set of volumes on Weld modeling by these authors.
11. F. W. Brust, I. S. Raju, and D. Cheston "Ares I-X USS Weld Residual Stress Analysis", NASA TM-xxxxx, 2008 (under final preparation).
12. Knight, N. F., Jr., Phillips, D. R., and Raju, I. S., *ARES I-X Upper Stage Simulator Structural Analyses Supporting the NESC Critical Initial Flaw Size Assessment*, NASA TM-2008-xxxxxx, 2008 (under final preparation).
13. Brust, F. W., and Scott, P. M., "Weld Residual Stresses and Primary Water Stress Corrosion Cracking in Bimetal Nuclear Pipe Welds", PVP 2007-26297, Proceedings of the ASME PVP 2007/Creep 8 Conference, ASME, July 22 - 26, 2007, San Antonio, Texas USA.
14. Scott, P. M., Brust, F. W., et al, "The Battelle Integrity of Nuclear Piping (BINP) Final Report", Nuclear Regulatory Commission Report NUREG/CR-6837, Vol. 1 and 2, Prepared by Battelle and Engineering Mechanics Corp., June, 2005.
15. D. S. Dawicke, I. S. Raju, and D. Cheston "Ares I-X USS Critical Initial Flaw Size Analysis", NASA TM-XXXXX, January 2007.
16. Cheston, D., et al, "Independent Evaluation of the Critical Initial Flaw Size for the Ares 1-X (AIX) Upper Stage Simulator (USS) Common Segment Flange-to-Skin Welds", NASA TM-XXXXX, January 2007.

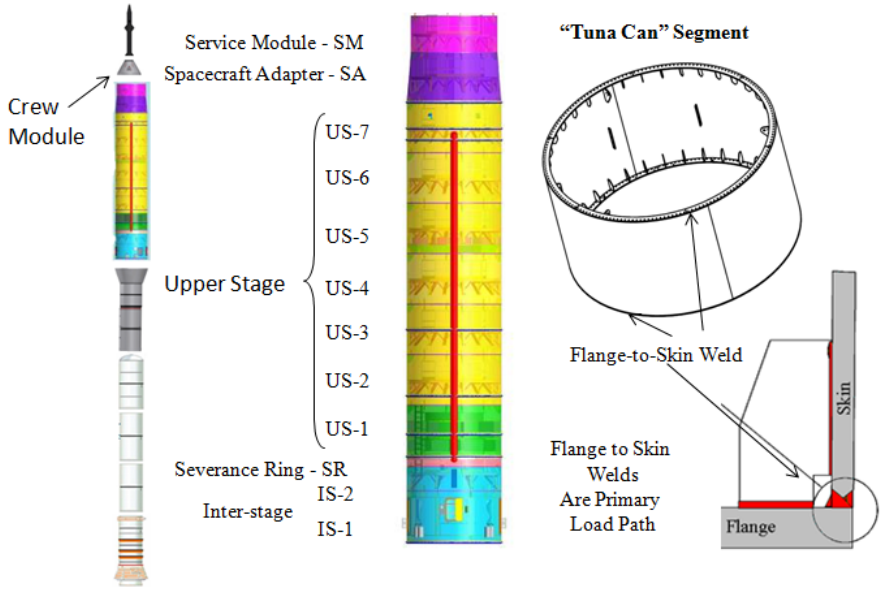

Figure 1. Ares I-X Upper Stage Simulator Critical Initial Flaw Size Assessment.

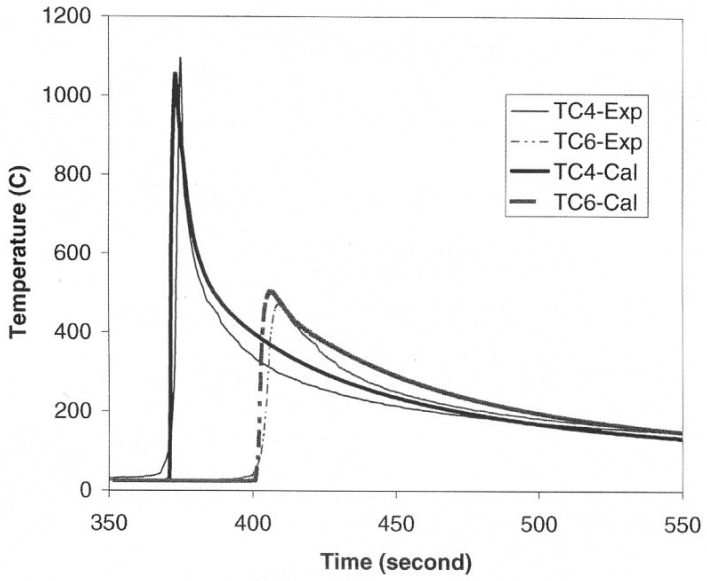

Figure 2. Validation Example for CTSP Thermal Analysis Code – Tee Fillet Weld.

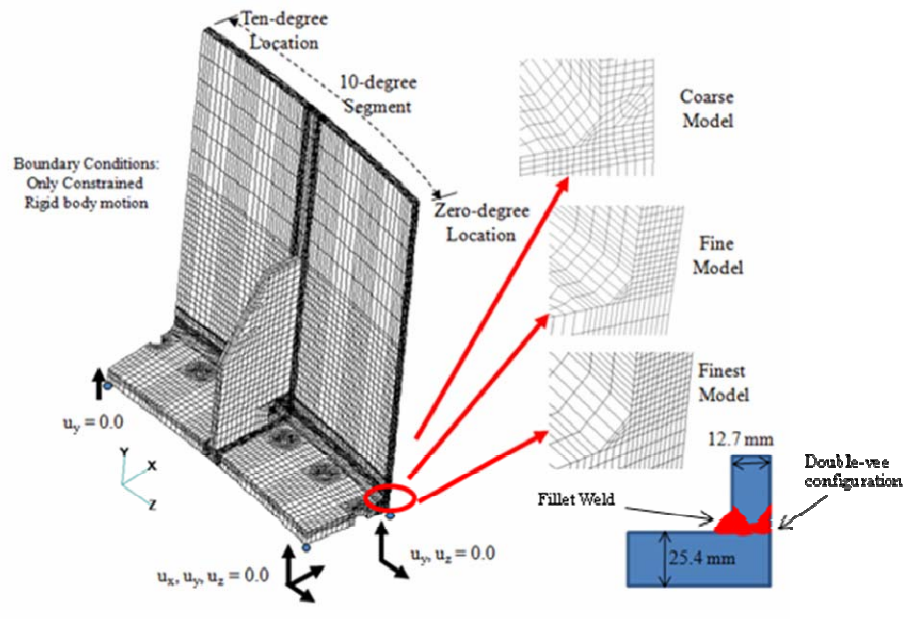

Figure 3 10-Degree Segment Model of Tuna Can Shell and Flange.

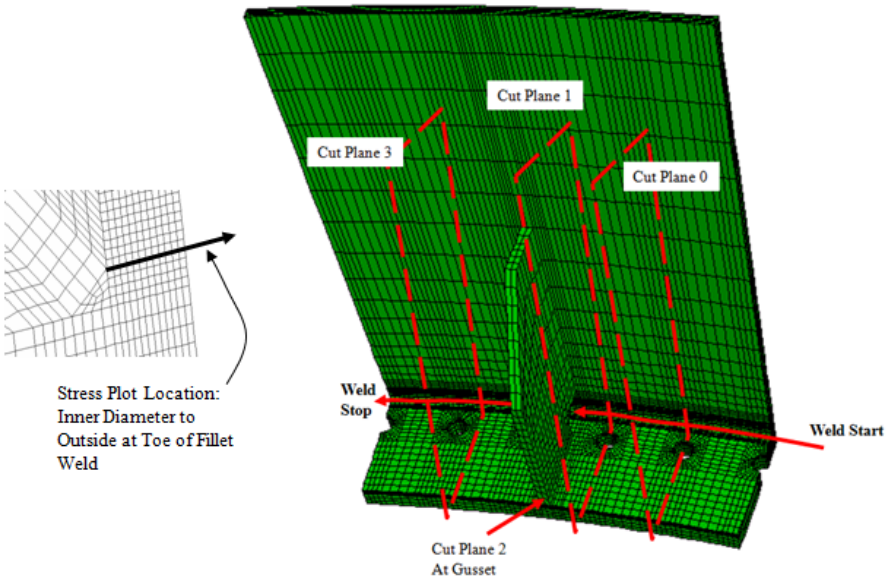

Figure 4 Cut Plane Definitions. Stresses are Plotted at These Locations.

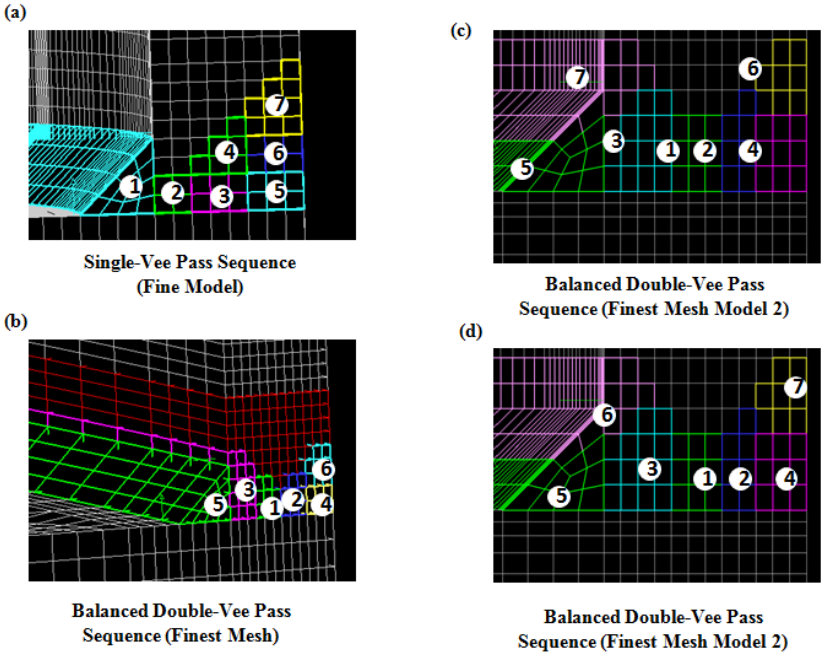

Figure 5 Weld Sequences Considered.

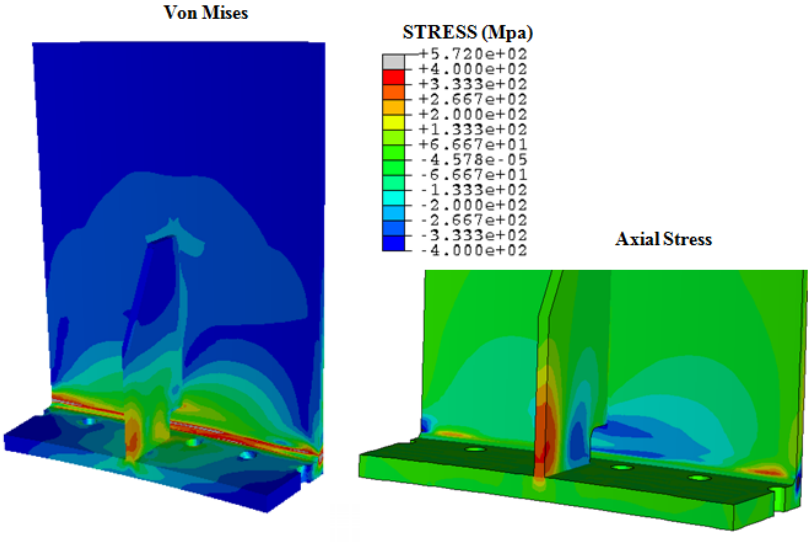

Figure 6 Weld Residual Stress Double-Vee (Von Mises and Axial) – Fine Model

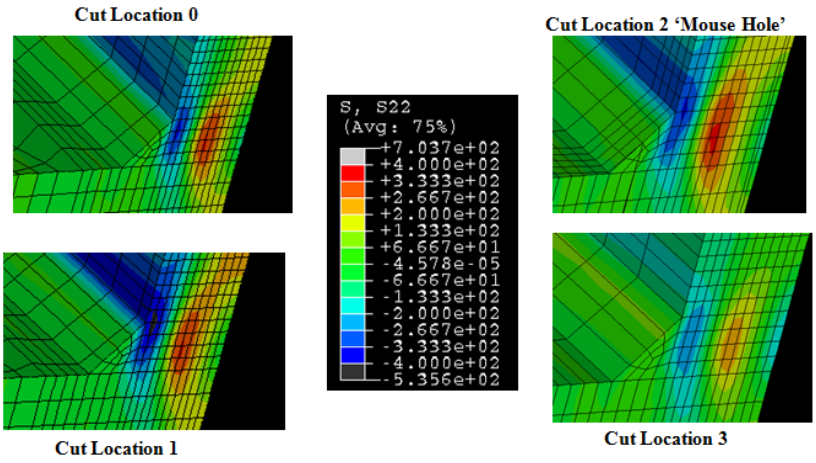

Figure 7 Axial Weld Residual Stress Double-Vee

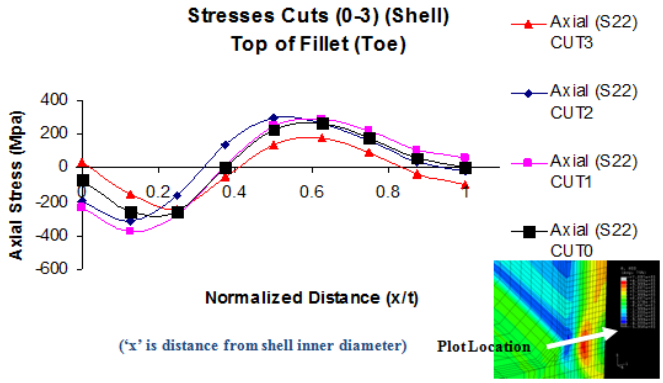

Figure 8 Line Plots of Axial Weld Residual Stress Double-Vee (finest mesh)

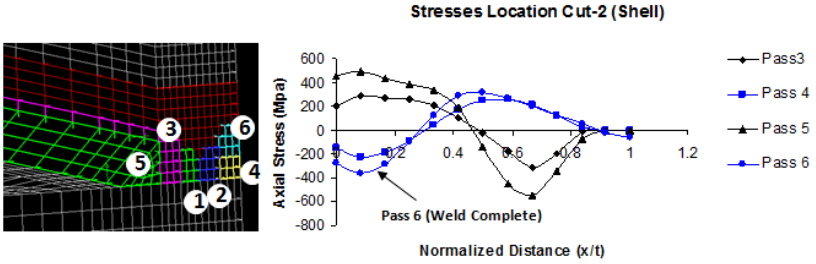

Figure 9. Weld Pass Effect on Axial Stress (Double Vee)

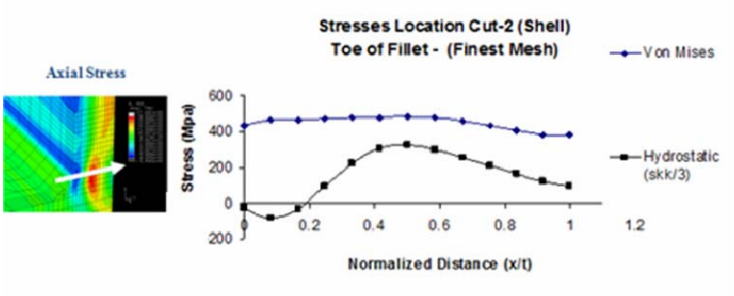

Figure 10. Constraint Effects and Weld Residual Stress

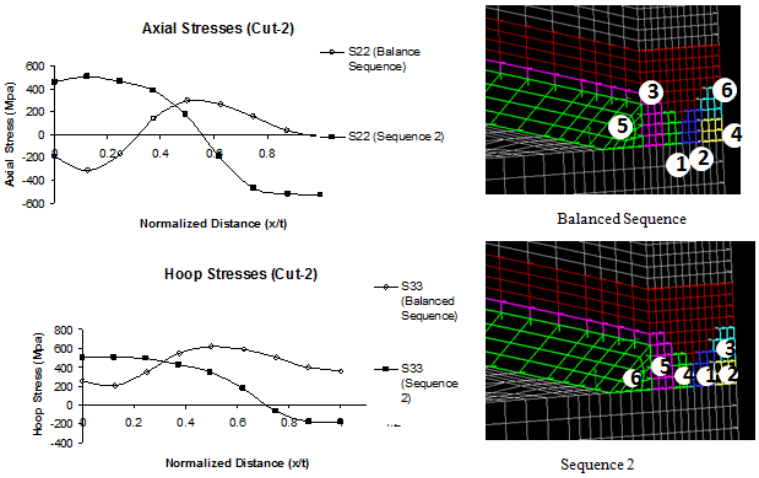

Figure 11. Effect of Weld Sequence (Cut-2 Location) Double-Vee

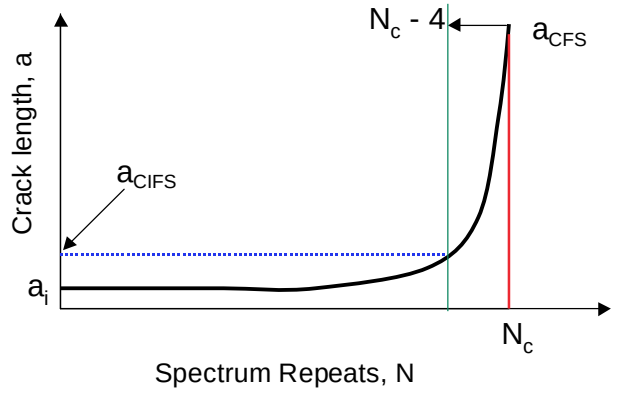

Figure 12. Schematic of the CIFS Approach.

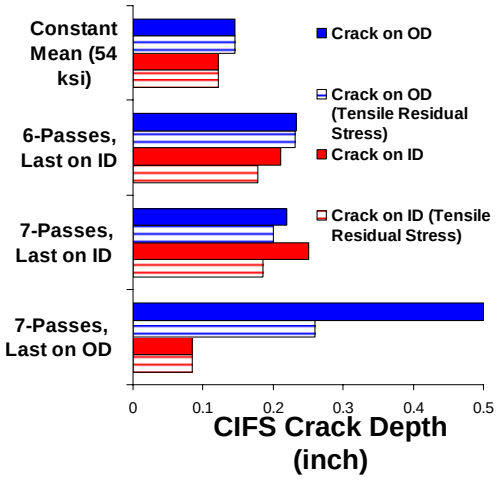

Figure 13. Results of the CIFS Assessment.